Available online at www.sciencedirect.com
ScienceDirect
Journal of Power Sources 160 (2006) 130–138
JOURNAL OF POWER SOURCES
www.elsevier.com/locate/jpowsour

A fundamental study of chromium deposition on solid oxide fuel cell cathode materials

Michael C. Tucker*, Hideto Kurokawa, Craig P. Jacobson, Lutgard C. De Jonghe, Steven J. Visco

Materials Sciences Division, Lawrence Berkeley National Laboratory, 1 Cyclotron Rd., MS 62-203, Berkeley, CA 94720, USA

Received 20 December 2005; received in revised form 1 February 2006; accepted 2 February 2006

Abstract

Chromium contamination of metal oxides and SOFC cathode catalysts is studied in the range 700–1000 °C. Samples are exposed to a moist air atmosphere saturated with volatile Cr species in the presence and absence of direct contact between the sample and ferritic stainless steel powder. Chromium contamination of the samples is observed to occur via two separate pathways: surface diffusion from the stainless steel surface and vapor deposition from the atmosphere. Surface diffusion dominates in all cases. Surface diffusion is found to be a significant source of Cr contamination for LSM and LSCF at 700, 800, and 1000 °C. Vapor deposition of Cr onto LSCF was observed at each of these temperatures, but was not observed for LSM at 700 or 800 °C. Comparison of the behavior for LSM, LSCF, and single metal oxides suggests that Mn and Co, respectively, are responsible for the Cr contamination of these catalysts.

Keywords: Solid oxide fuel cell; Stainless steel; Chromium; LSM; LSCF

1. Introduction

The possibility of a metal-supported SOFC with ferritic stainless steel interconnects, cathode current collector, and balance of plant components is particularly alluring because of the low cost and fuel flexibility such a system may offer. Previous generations of SOFC technology have utilized cells produced entirely of ceramic components on the air side, with Ni as the catalyst and current collector on the fuel side. Limiting the presence of ceramic components to thin active layers, while utilizing stainless steel for the cell support, current collection, and interconnection results in a robust and cost-competitive SOFC stack. Introducing stainless steel to the cell materials set, however, presents new challenges that must be overcome. Of particular concern is performance degradation due to interactions between the stainless steel components and catalysts. Chromium contamination of SOFC cathodes operating in the presence of stainless steel interconnects has been observed repeatedly in the literature [1–6]. The mechanism of contamination has yet to be clarified, and the effects of temperature and catalyst surface chemistry on Cr deposition are not yet well understood. This paper presents initial findings of a fundamental study intended to elucidate the details of Cr contamination of SOFC cathodes. The main purposes of this work are to assess the relative roles of vapor deposition and surface diffusion of Cr, and determine which individual metal oxides are likely responsible for Cr contamination of mixed oxide catalysts.

In moist air, the Cr_2O_3 scale on stainless steel SOFC and balance of plant components generates a significant vapor pressure of volatile hexavalent Cr species, including CrO_3 and $CrO_2(OH)_2$ [7–9]. The partial pressures of CrO_3 and $CrO_2(OH)_2$ are independent of, and directly dependent on moisture content, respectively. The dominant species in moist air is $CrO_2(OH)_2$. Localized reduction can cause these species to deposit onto the cathode. In the case of a stainless steel interconnect or current collector directly contacting the SOFC cathode, local Cr vapor pressures can approach saturation, and therefore significant Cr vapor deposition can be envisioned. Even in the absence of a stainless steel interconnect or current collector in the cathode compartment, upstream components such as manifolds and heat exchangers can produce significant contamination of the cathode air feed with volatile Cr species. One would also expect surface

* Corresponding author. Tel.: +1 510 486 5850; fax: +1 510 486 4881.
E-mail address: mctucker@lbl.gov (M.C. Tucker).

0378-7753/$ – see front matter © 2006 Elsevier B.V. All rights reserved.
doi:10.1016/j.jpowsour.2006.02.017

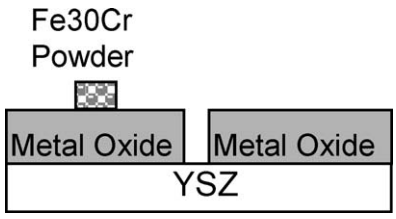

Fig. 1. Schematic of sample geometry. Samples were exposed to Cr-saturated atmosphere.

diffusion of Cr species from the Cr_2O_3 scale onto the cathode catalyst wherever there is physical contact between the two. Both vapor deposition and surface diffusion are plausible sources of Cr contamination. This work separates the two by exposing various metal oxides to a Cr-saturated atmosphere, both with and without direct contact to Cr_2O_3-forming stainless steel particles. The degree of Cr contamination in the presence and absence of stainless steel contact is then determined, providing a qualitative assessment of the relative importance of vapor deposition and surface diffusion for each metal oxide.

Various mechanisms for Cr contamination of SOFC cathode materials have been proposed in the literature. These include electrochemical reduction of volatile Cr species at the active cathode sites [1,2], chemical deposition due to low oxygen partial pressure near the active sites [1,3,5], and enhanced chemical deposition due to formation of Mn^{2+} at the electrolyte interface [5]. In each case, we presume that the depositing Cr species will display an affinity for particular chemical species on the surface of the catalyst, and therefore expect that pairwise interaction between Cr species and individual metal oxides dominates the contamination behavior of mixed catalyst oxides. To ascertain which individual metal oxides are responsible for promoting Cr deposition onto cathode catalyst materials, vapor deposition and surface diffusion of Cr onto single element oxides were observed. Comparing the results to similar observations of typical cathode catalysts allows a phenomenological determination of the particular metals that dominate contamination of the mixed oxide catalyst surface. We anticipate the use of this information in designing a catalyst material that is tolerant to the presence of Cr, and in determining other strategies for reducing the impact of Cr contamination on cathode performance.

2. Experimental methods

Single element oxide samples were prepared on YSZ substrates in the geometry indicated in Fig. 1. Substrates were prepared by sintering YSZ (Tosoh 8Y) in air at 1400 °C for 4 h. The oxides were applied by melting metal nitrates onto the YSZ substrate and then firing to 800 °C in air to convert the nitrate to oxide. The resulting oxide layers were continuous and porous. Cathode catalyst samples were prepared by spraying two thin regions of catalyst powder onto YSZ substrates and firing at 1200 °C in air for 2 h. Three catalyst compositions were used (Praxair): "LSM6530" ($La_{0.65}Sr_{0.30}MnO_3$), "LSM8515" ($La_{0.85}Sr_{0.15}MnO_3$), and "LSCF" ($La_{0.6}Sr_{0.4}Co_{0.2}Fe_{0.8}O$). Each oxide and catalyst sample consisted of two separate regions, one of which was contacted with a small amount of Fe30Cr stainless steel powder (Ametek). Pellets of Mn_2O_3 and Mn_3O_4 powders (Aldrich) were also prepared by pressing with HPC (Klucel) as binder. Small stainless steel powder contacts were applied to the pellets before exposure testing. Stainless steel powder contacts were not oxidized prior to sample exposure testing.

The oxidation state of Mn in manganese oxide changes rapidly with temperature in the vicinity of 800 °C. Therefore, X-ray diffraction (XRD, Siemens Kristalloflex) was used to determine the phases present after conversion of the nitrate to oxide and after exposure testing at 800 °C. In both cases, Mn_2O_3 was the predominant phase, with minor Mn_3O_4 detected. Minor MnO_2 was additionally detected after exposure testing. This manganese oxide is therefore referred to as "MnO_x" throughout the text.

Specimens were exposed to flowing gas saturated with volatile Cr species at different temperatures for 150 h. The glassware setup is described elsewhere [8]. The various experimental conditions are listed in Table 1. The partial pressures of volatile Cr species were calculated using thermodynamic values reported by Ebbinghaus [10]. Chromium saturation of the gas was assured by placing the specimens downstream of several high-surface area pieces of Cr_2O_3. The partial pressure of volatile Cr species directly depends on the oxygen and moisture content of the atmosphere, and is weakly thermally activated, changing less than an order of magnitude over the range 700–1000 °C [10,11]. By controlling the oxygen pressure and moisture dewpoint in the flowing gas, the partial pressure of the Cr species was controlled. Moisture content was controlled by bubbling the flowing gas through water held at the dewpoint temperature upstream of the specimen chamber inlet. In moist conditions, $CrO_2(OH)_2$ is the dominant Cr vapor species, and its partial pressure was held constant in all experiments. CrO_3 is a secondary Cr vapor species, and increases the total volatile Cr pressure to a minor extent at 1000 °C. Samples were also exposed to dry atmosphere at 1000 °C, in which CrO_3 is the dominant volatile species. Throughout the text, exposure at 1000 °C is in moist atmosphere, unless otherwise noted.

Post-exposure SEM/EDS analysis was conducted with a Hitachi S4300 microscope.

Table 1
Experimental conditions of Cr-saturated atmosphere for various 150 h exposure runs

T (°C)	P_{O_2} (atm)	H_2O dewpoint (°C)	P_{H_2O} (atm)	$\log(P_{CrO_2(OH)_2})$ (atm)	$\log(P_{Cr}$ total) (atm)
700	0.2	42.4	0.083	−6.34	−6.34
800	0.2	33.1	0.050	−6.34	−6.34
1000	0.14	25.0	0.031	−6.34	−6.26
1000	0.14	Dry	–	–	−7.04

3. Results and discussion

3.1. Chromium contamination of single element metals and oxides

Single element oxides with and without contact by stainless steel particles were exposed to an atmosphere saturated with Cr species. One set of samples was exposed to moist air at 800 °C for 150 h (see Table 1). After this exposure, the extent of Cr vapor deposition and surface diffusion were determined by SEM and EDS analysis. Chromium contamination in the absence of stainless steel contact is presumed to occur by direct vapor deposition, whereas contamination very near the contact is presumed to occur by surface diffusion of Cr from the stainless steel surface. The extent of Cr contamination depends strongly on the identity of the substrate. The metals and oxides studied can be divided into three general classes according to their Cr contamination behavior: (a) minimal surface diffusion, minimal vapor deposition; (b) significant surface diffusion, significant vapor deposition; and (c) significant surface diffusion, minimal vapor deposition. An example of each class will be presented in some detail below, followed by a summary of the results for all elements studied.

Fig. 2 shows the EDS spectra for a ZrO_2 sample after exposure. Three regions of interest were analyzed: near the stainless steel contact (<50 μm from edge of stainless steel); far from the stainless steel (>1 mm from edge of stainless steel); and a separate sample with no stainless steel contact. No Cr was detected far from the stainless steel or with no stainless steel contact. Thus, Cr vapor deposition onto ZrO_2 was not observed. Near the stainless steel, a trace amount of Cr was detected, indicating that minimal surface diffusion of Cr occurs on ZrO_2.

The behavior of Co_3O_4 is quite different. Fig. 3a shows the EDS spectra after exposure. Chromium is readily detected both far from the stainless steel and with no stainless steel contact. This indicates that significant vapor deposition of Cr onto Co_3O_4 occurs. A very large amount of Cr is detected near the stainless steel contact, as a result of significant surface diffusion of Cr onto the oxide. Fig. 3b shows the ratio of Cr and Co EDS signal strength as a function of distance from the stainless steel surface. The data are noisy due to the uneven surface of the sample, but the trend is clear. Vapor deposition provides a baseline of Cr contamination far from the stainless steel, whereas surface diffusion dominates near the stainless steel contact. Chromium provided by surface diffusion is present many hundreds of micrometers away from the stainless steel contact, suggesting a high Cr surface-migration rate of several micrometers per hour. Fig. 4 shows SEM images of the oxide surface. Far from the stainless steel contact, the morphology is characterized by submicrometer-size crystals that are somewhat faceted. In contrast, large well-developed crystals are observed near the stainless steel contact. Such crystals are consistent with the formation of $Co_{3-x}Cr_xO_4$ spinel, which is stable over a wide range of Cr contents [12].

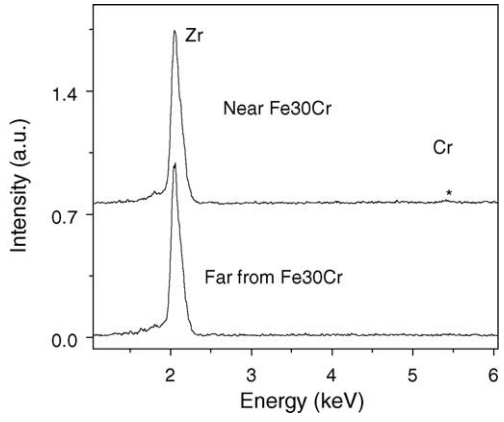

Fig. 2. EDS spectra for ZrO_2 samples conditioned 150 h in 800 °C moist air. Upper data are shifted vertically for clarity.

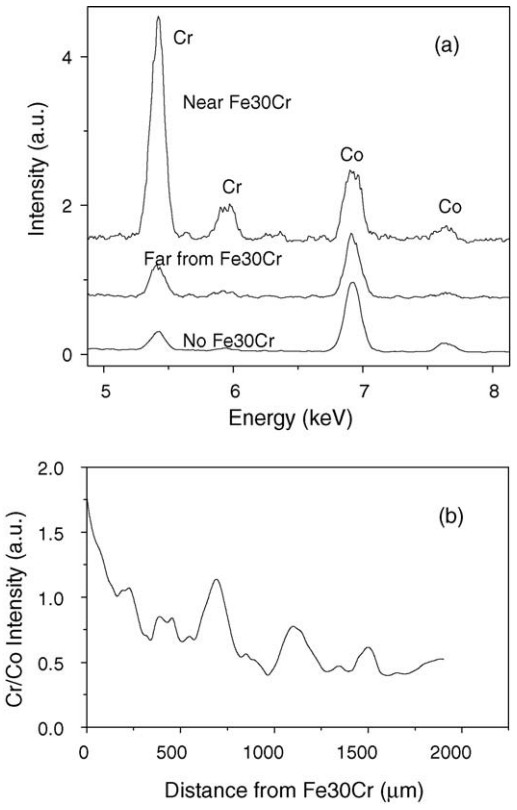

Fig. 3. (a) EDS spectra for Co_3O_4 samples conditioned 150 h in 800 °C moist air. Upper data are shifted vertically for clarity. (b) Cr/Co EDS signal intensity ratio along a line extending over the Co_3O_4 surface from the edge of the contacting stainless steel powder.

MnO_x also supports significant Cr surface diffusion, as indicated by the large amount of Cr detected near the stainless steel contact, Fig. 5a. A very small amount of Cr is detected far from the stainless steel, and only a trace amount is detected in the case of no stainless steel contact. Thus, vapor deposition of Cr onto MnO_x is seen to be minor. Fig. 5b shows the ratio of Cr and Mn EDS signal strength as a function of distance from the stainless steel surface. There is a clear band of significant Cr contamination extending about 200 μm from the stainless steel surface. Outside this band, minor Cr from vapor deposition is detected. The edge of the Cr surface diffusion band is much sharper on MnO_x than on Co_3O_4; this distinction may arise from differences

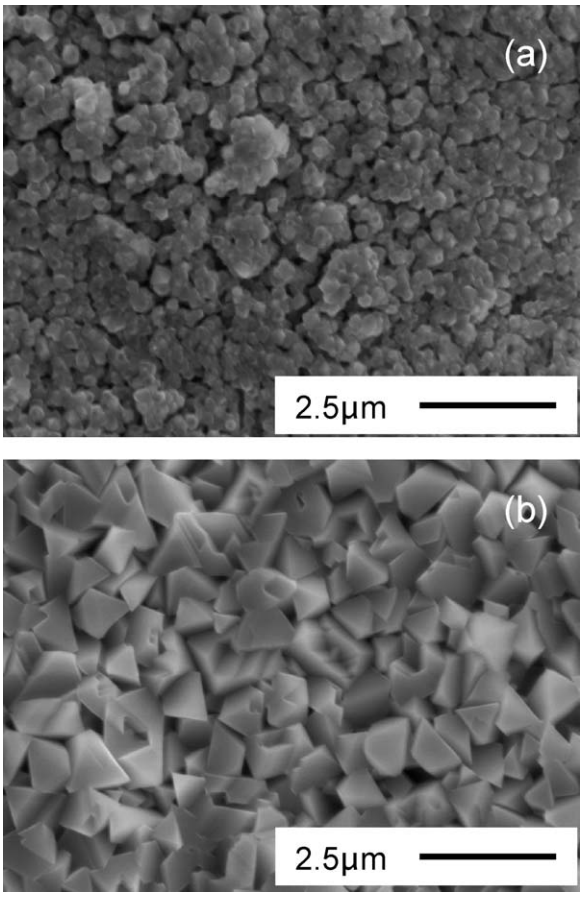

Fig. 4. SEM images of the Co_3O_4 surface after conditioning 150 h in 800 °C moist air. (a) No stainless steel contact and (b) near stainless steel contact.

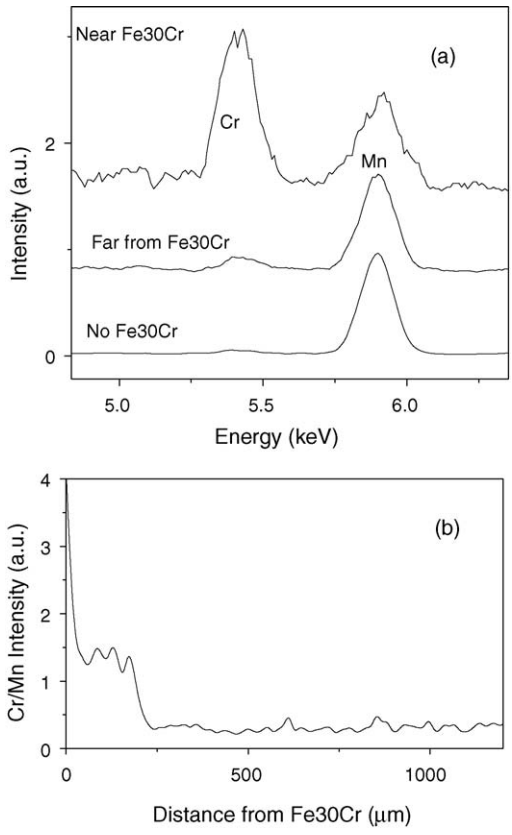

Fig. 5. (a) EDS spectra for MnO_x samples conditioned 150 h in 800 °C moist air. Upper data were shifted vertically for clarity. (b) Cr/Mn EDS signal intensity ratio along a line extending over the MnO_x surface from the edge of the contacting stainless steel powder.

in the mechanism of Cr transport on these oxides. In particular, $Co_{3-x}Cr_xO_4$ is a stable solid solution for a continuous range of Cr contents, whereas $Mn_xCr_{3-x}O_4$ is stable only for x greater than 0.5 [12,13]. The band of Cr-rich phase is clearly visible around the stainless steel particle contact, Fig. 6. Outside this band, the morphology is characterized by small, irregular particles, Fig. 6a. Large, well-developed crystals are observed inside this band near the stainless steel contact. The shape of the crystals is consistent with that reported previously for $Mn_xCr_{3-x}O_4$ spinel [13].

Chromium deposition was also observed on pellets of MnO_x powder after 150 h exposure at 700 or 1000 °C. After conditioning, the stainless steel powder contact was removed from the pellets to allow SEM/EDS analysis of the pellet surface under the stainless steel. XRD was used to determine the MnO_x phases present after conditioning. The 700 °C sample contained predominantly Mn_2O_3 with minor Mn_3O_4 impurity, implying an average Mn oxidation state of roughly Mn^{3+}. The 1000 °C sample was predominantly Mn_3O_4, with minor Mn_2O_3 impurity, indicating a mixture of Mn^{2+} and Mn^{3+}. This lowered Mn oxidation state is interesting because the literature suggests that Cr contamination of LSM is promoted by localized reduction which produces Mn^{2+} near the LSM/electrolyte interface [5]. Fig. 7 shows the dramatic difference in Cr deposition at 700 and 1000 °C. Comparing Fig. 7a and b, it can be seen that large

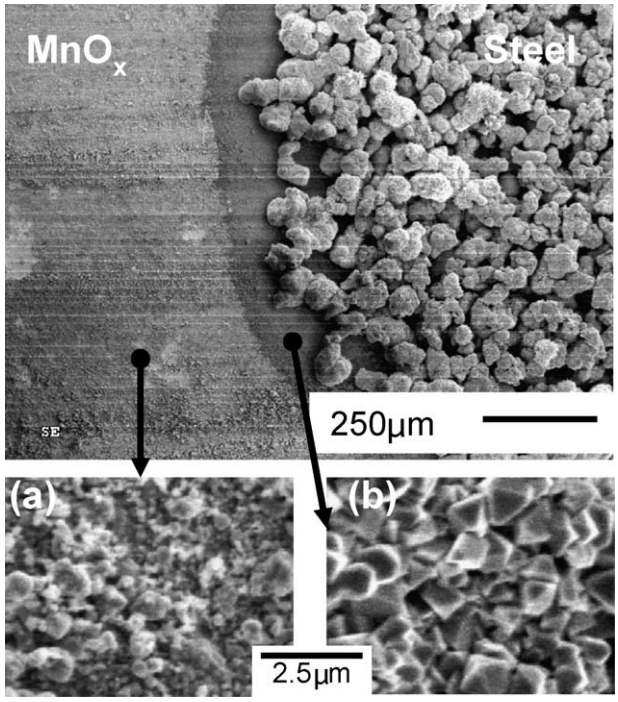

Fig. 6. SEM images of the MnO_x surface after conditioning 150 h in 800 °C moist air. Note the ring of highly Cr-contaminated MnO_x surrounding the stainless steel. High magnification images show the MnO_x surface (a) outside and (b) in this ring.

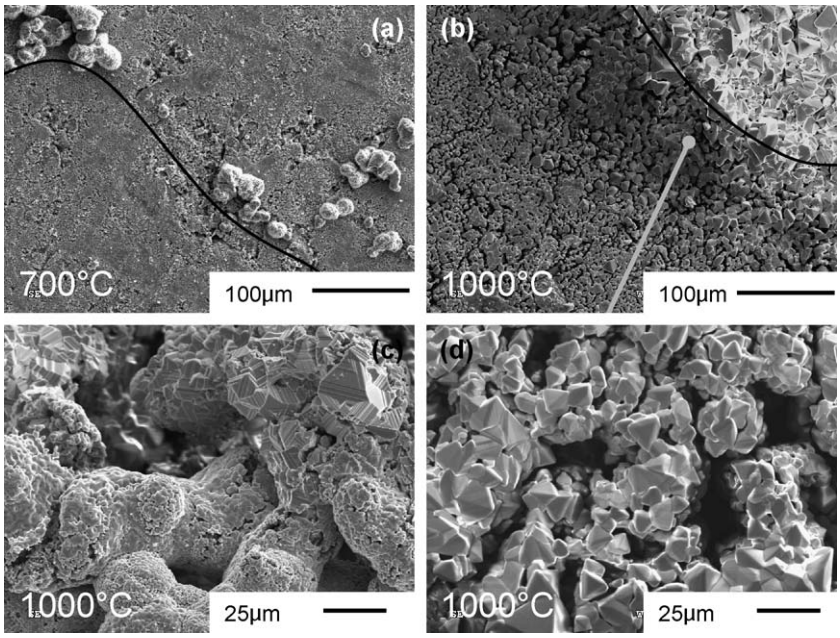

Fig. 7. SEM images of the surface of MnO_x pellets after exposure to Cr-saturated atmosphere in the presence of stainless steel contact at (a) 700 °C and (b–d) 1000 °C. Stainless steel contact particles were present to the right of the lines in images (a) and (b) during exposure and were then removed after exposure to reveal the MnO_x surface beneath. The edge of the stainless steel contact nearest the MnO_x surface is shown before removal in (c). A highly Cr-contaminated band is visible just outside the stainless steel contact area in image (b); an enlargement of this area is shown in (d).

faceted crystals have grown under and around the stainless steel contact at 1000 °C whereas there is no visual evidence of Cr surface diffusion at 700 °C. Fig. 7d shows a high-magnification image of the pellet surface near the stainless steel contact; the crystal shape is consistent with the presence of $Mn_xCr_{3-x}O_4$ spinel. Fig. 7c shows the stainless steel powder surface near the edge of the stainless steel contact before it was removed from the pellet. The large spinel-like crystals were determined by EDS to contain a high amount of Mn. Some Mn from the pellet reacted with the stainless steel, probably by surface or bulk diffusion of Mn through the stainless steel. We presume that this migration of Mn affects the oxidation behavior of the stainless steel. Mn was not detected in the stainless steel powders after conditioning at 700 or 800 °C. The EDS data in Fig. 8 confirm that surface diffusion and vapor deposition of Cr onto MnO_x are significantly enhanced at 1000 °C relative to 700 °C. Bearing in mind that the 700 and 1000 °C experiments were conducted with essentially constant partial pressure of Cr species in the atmosphere, the marked thermal activation of Cr contamination probably arises from thermal activation of the surface diffusion and vapor deposition kinetics. We furthermore presume that partial reduction of Mn^{3+} to Mn^{2+} may be contributing to the high Cr deposition rates observed at 1000 °C.

Chromium contamination of several other single oxides, metals, and bulk ceramics was observed at 800 °C. The results are summarized in Table 2. The behavior for each was qualitatively similar to that of ZrO_2, Co_3O_4, or MnO_x. SrO is the only other single oxide studied that, like Co_3O_4, displays significant vapor deposition of Cr. No oxides were found that support vapor deposition but not surface diffusion of Cr. In fact, greater Cr concentrations were detected near the stainless steel contact for all samples studied. Clearly, surface diffusion of Cr must always be accounted for when analyzing Cr-based cathode degradation or designing a cathode that is tolerant to the presence of Cr. Further studies are under way to determine the mechanism of Cr surface diffusion.

None of the precious metals studied display Cr vapor deposition, and only gold supports significant surface diffusion of Cr. These results should be considered when choosing a precious metal contact for current collection in a SOFC test cell. For instance, if Pt or Ag is placed between a cathode and Cr source, surface diffusion of Cr onto the cathode could be inhib-

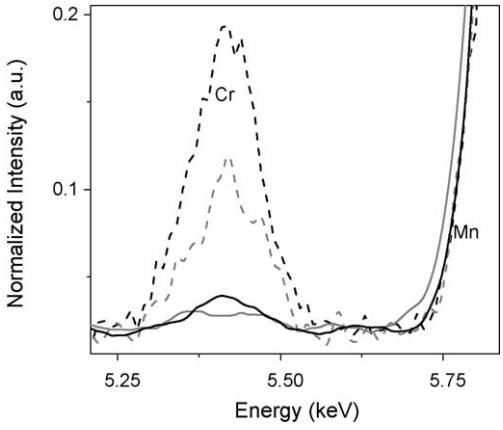

Fig. 8. EDS spectra for MnO_x pellets after Cr contamination. Spectra have been normalized to the Mn peak. Two areas are represented: (dashed lines) under the stainless steel contact (contact was removed before EDS analysis) and (solid lines) far from the stainless steel contact. (Black lines) 1000 °C moist atmosphere; (gray lines) 700 °C moist atmosphere.

Table 2
Summary of Cr contamination results after exposure at 800 °C for 150 h

	Surface diffusion	Vapor deposition
Single oxide		
Ca	Observed	Trace
Ce	Trace	Not detected
Co	Significant	Significant
Cu	Observed	Not detected
Fe	Observed	Not detected
Ga	Observed	Observed
Gd	Observed	Trace
La	Observed	Not detected
Mg	Significant	Observed
Mn	Significant	Trace
Ni	Trace	Not detected
Pr	Observed	Not detected
Sc	Trace	Not detected
Sm	Observed	Trace
Sr	Significant	Significant
Y	Observed	Trace
Zr	Trace	Not detected
Metal		
Ag	Trace	Not detected
Au	Significant	Not detected
Pt	Trace	Not detected
Bulk ceramic		
Al_2O_3	Trace	Trace
TiO_2	Trace	Not detected
Electrolyte		
YSZ*	Trace	Not detected
CGO*	Trace	Not detected
LSGM*	Observed	Observed
Mixed oxide		
LSM6530	Significant	Not detected
LSM8515	Significant	Not detected
LSCF	Significant	Significant

* Electrolyte compositions exposed at 1000 °C.

ited. If Au is used, it may provide a path for enhanced Cr transport.

3.2. Chromium contamination of electrolyte and cathode mixed oxides

Three electrolyte compositions, YSZ, CGO, and LSGM, were tested for Cr contamination at 700 and 1000 °C. Each electrolyte material showed only minor surface diffusion and no vapor deposition of Cr at 700 °C. The same results were obtained for YSZ and CGO at 1000 °C. For both YSZ and CGO the main constituent, ZrO_2 and CeO_2, respectively, displayed only minor surface diffusion of Cr (Table 2), whereas minor vapor deposition was additionally observed for the dopants, Y_2O_3 and Gd_2O_3, respectively. At low dopant levels, the dopant clearly has minimal impact on the Cr contamination behavior of the bulk electrolyte material. The Cr contamination behavior is probably determined by the surface composition, which may differ from the bulk dopant level. Both surface diffusion and vapor deposition of Cr was observed for LSGM at 1000 °C. This is consistent with the results at 800 °C for the constituent oxides: La_2O_3, SrO, Ga_2O_3, and MgO all promote surface diffusion of Cr, and all except La_2O_3 promote vapor deposition of Cr. Importantly, reduction of the temperature from 1000 to 700 °C practically eliminates Cr contamination for these electrolytes.

LSCF and two compositions of LSM were exposed to stainless steel contact and Cr-saturated atmosphere for 150 h at 700, 800, and 1000 °C. Fig. 9 shows the EDS spectra for 800 and 1000 °C after exposure. Two peaks at 5.1 and 5.38 keV are assigned to La, and the latter is overlapped by the strongest Cr peak. At 800 °C, both LSM compositions show Cr contamination near the stainless steel contact, arising from surface diffusion. Neither composition shows detectable vapor deposition of Cr in the absence of stainless steel contact. The spectra have been normalized to the La peak at 5.1 keV, so the larger Cr signal for LSM6530 is partly due to the lower La concentration of that sample. Both LSM compositions show similar behavior. Furthermore, the surface composition of LSM does not change dramatically with bulk composition for Sr contents of interest [14]. Control of LSM stoichiometry is, therefore, probably not a fruitful path for significantly reducing Cr diffusion. Significantly more Cr surface diffusion is observed for LSCF. In contrast to LSM, there is also a small but clearly detectable Cr peak in the absence of stainless steel contact arising from vapor deposition onto LSCF. For all three compositions, the results for 700 °C exposure were qualitatively similar to those for 800 °C, although significantly less Cr contaminated the samples at the lower temperature. At 1000 °C, however, the nature of Cr contamination changes. Vapor deposition of Cr is observed for both LSM compositions, and the extent of vapor deposition onto LSCF has increased significantly. Because the partial pressure of Cr in the atmosphere was held essentially constant at all three exposure temperatures, these results suggest that vapor deposition is more thermally activated than surface diffusion. These data also clearly show that Cr contamination occurs via a chemical mechanism, although an additional electrochemical pathway for Cr deposition cannot be ruled out.

The dependence of Cr vapor deposition on temperature is further demonstrated in Fig. 10. Images of the LSM and LSCF samples with no stainless steel contact are shown after exposure at 700, 800, and 1000 °C. Large faceted crystals are observed on LSCF at all temperatures studied, whereas crystals are only observed on LSM at 1000 °C, consistent with the EDS analysis above. Table 1 shows that at 1000 °C there is a small increase in the total pressure of Cr species, due to CrO_3 which is essentially not present at 700 or 800 °C. It could be argued that vapor deposition of CrO_3 is so much faster than $CrO_2(OH)_2$ that the low CrO_3 partial pressure would be solely responsible for the crystal growth observed at 1000 °C. This possibility was ruled out, however, by repeating the experiment in a dry atmosphere; the same pressure of CrO_3 was achieved, yet essentially no $CrO_2(OH)_2$ was evolved. While, in this case, a small extent of Cr vapor deposition was still observed on LSM, it was not enough to form crystals.

For fixed oxygen and water vapor pressures, the partial pressure of Cr is relatively invariant with temperature [10]. From this thermodynamic standpoint, one might argue that the Cr contamination problem cannot be solved by simply lowering the

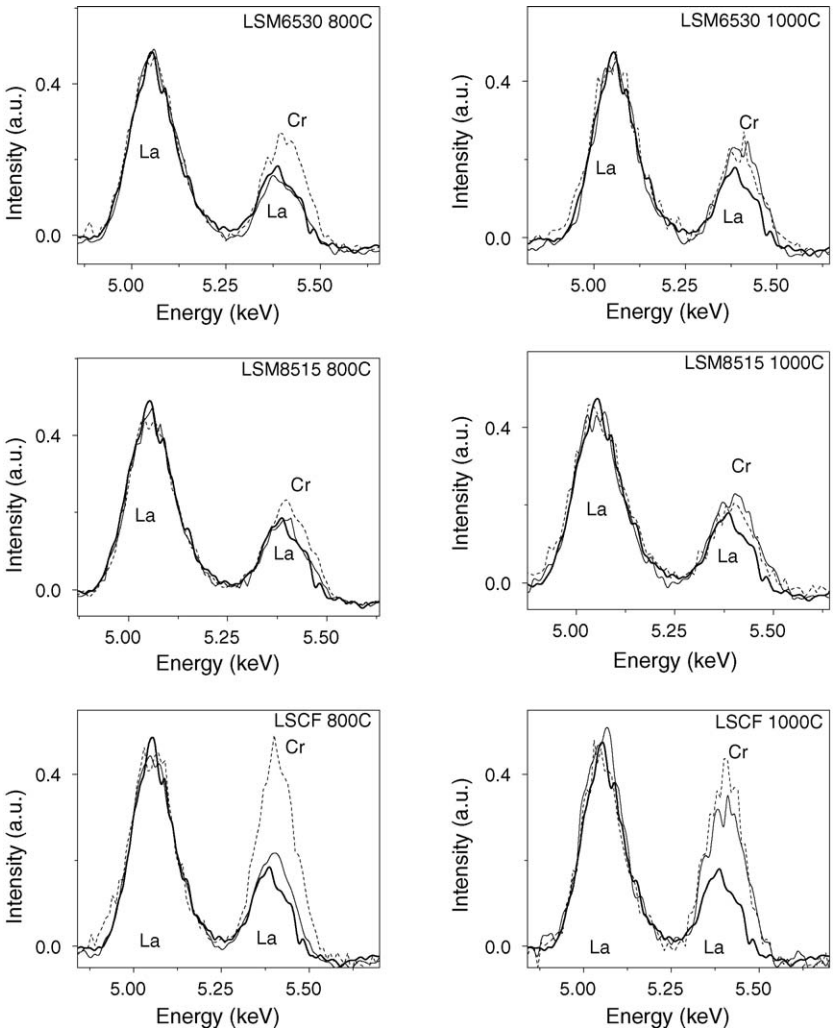

Fig. 9. EDS spectra for LSM and LSCF after Cr contamination at 800 and 1000 °C. Spectra are shown for La background signal (thick line), near stainless steel contact (dashed line) and in the absence of stainless steel contact (thin line). Spectra are normalized to the La peak at 5.1 keV.

SOFC operating temperature. The data presented here, however, clearly show that Cr contamination via a chemical mechanism is quite thermally activated. It is not yet clear why this is the case, but thermally activated contamination kinetics or reduction of the perovskite transition metal oxidation state with increased temperature are both plausible explanations. Many studies of SOFC cathode poisoning by Cr contamination have been carried out at high temperature (900–1000 °C) [1,3,5,6], and we are not aware of any work that has determined the extent of Cr contamination in the vicinity of 700 °C. Yet the target operating temperature range for long-term stability of SOFCs with stainless steel components is below 750 °C [15]. Because Cr contamination is found to be strongly temperature-dependent, there is a need to address the behavior of cathode catalysts operating in the presence of stainless steel components at lower temperatures.

Comparing the qualitative behavior of LSM, LSCF, and the single element oxides (Table 2) allows us to deduce which elements are responsible for the contamination of the complex oxides. Because LSM does not show vapor deposition at 800 °C, yet SrO does, we surmise that La or Mn dominate the Cr contamination behavior. Likewise LSCF does display Cr deposition from the vapor phase at 800 °C, so we surmise that Sr or Co dominate the Cr contamination behavior. Furthermore, both LSM and LSCF contain La and Sr yet display qualitatively different Cr contamination behavior, so we suspect that Mn and Co are ultimately responsible for Cr deposition onto these mixed oxides.

3.3. Effects on oxidation of stainless steel

As Cr-containing stainless steel oxidizes, a protective Cr_2O_3 scale grows and the surface becomes enriched in Cr. This was easily detected with EDS analysis of the stainless steel surface: fresh stainless steel displays a Cr/Fe surface atomic ratio of ~0.5, whereas after 150 h oxidation in air at 800 °C the ratio increases to ~6. Stainless steel contact particles were added to the oxide samples in the as-received state (i.e. not pre-oxidized). After oxidation in contact with the single oxides during Cr exposure testing, the stainless steel Cr/Fe ratio was in the range 0.5–3.5 for all oxides except Ni and Ce. This depression of the surface Cr concentration suggests that the presence of the oxides affects

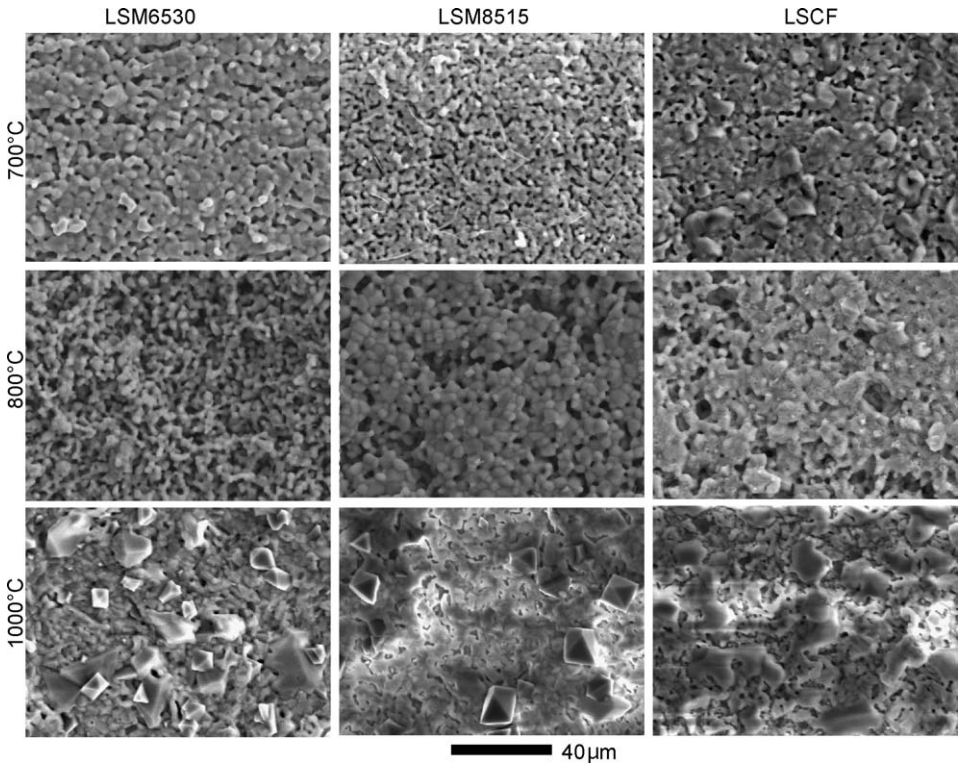

Fig. 10. SEM images of mixed perovskite surfaces after exposure to Cr-saturated atmosphere in the absence of stainless steel contact. Exposure temperatures are indicated on the left of the images; other exposure conditions are listed in Table 1.

the scale formation on the stainless steel. We presume the dominant mechanism is simple depletion of Cr from the stainless steel scale as Cr diffuses out onto the surface of the oxide sample. Therefore, it may be desirable to pre-oxidize any stainless steel that will directly contact the cathode material to form a surface scale that can function as a Cr reservoir; otherwise Cr-depletion to the extent of interfering with initial scale continuity may be a concern. A secondary mechanism that can affect scale growth is diffusion of metal cations from the single metals or oxides into the stainless steel. For most oxides studied, the stainless steel particles contained only Cr and Fe after oxidation at 800 °C in contact with the oxide. A few particular metal cations diffused from the oxide into the stainless steel, however, and were detected at the stainless steel surface farthest from the contact point with the oxide. The atomic concentrations of these elements determined by EDS were: Ca, 3%; Ag, 7%; Y, 3%; La, 1%. The presence of these elements may affect long-term oxidation of the stainless steels.

Pre-oxidation is expected to lower the rate of metal cation diffusion from the oxide into the steel. The significant diffusion of Mn from MnO_x into stainless steel at 1000 °C (discussed in Section 3.1) is possibly a concern for Mn-containing catalysts such as LSM. When operating in contact with a stainless steel current collector or interconnect, Mn may be depleted from the catalyst. In fact, Mn-migration into stainless steel was observed for stainless steel in contact with LSM at 1000 °C, but not at 700 or 800 °C. This Mn-migration at 1000 °C was accompanied by Mn-depletion of the LSM near the stainless steel contact. The Mn/La atomic ratio was 58% lower in the vicinity of the stainless steel contact than it was far away from the stainless steel contact. No such Mn-depletion was observed at 700 or 800 °C, suggesting that it is not a concern for stability of SOFCs operating at a temperature range appropriate for the use of stainless steel components (<750 °C). Neither Mn-migration into the stainless steel nor Mn-depletion of the nearby LSM was observed at 1000 °C in dry atmosphere, indicating that moisture is necessary for this Mn transport to occur. We speculate that modification of the LSM composition as Mn diffuses into contacting stainless steel may contribute to the high-temperature cathode degradation reported in the literature [1,3,5].

4. Conclusions

Single element and mixed element oxides were exposed to an atmosphere saturated with volatile Cr species in the presence and in the absence of direct contact between the oxides and the stainless steel powder. This allowed analysis of two separate pathways for Cr contamination: surface diffusion from the stainless steel surface and vapor deposition from the atmosphere. The extent to which these pathways caused Cr contamination varied considerably with the identity of the oxide substrate. The amount of contamination was thermally activated and surface diffusion provided a higher degree of Cr contamination than vapor deposition for all cases studied. This should be accounted for when analyzing Cr-based cathode degradation or developing strategies to reduce the impact of Cr contamination.

Surface diffusion was found to be a significant source of Cr contamination for LSM and LSCF at 700, 800, and 1000 °C. Vapor deposition of Cr onto LSCF was observed at each of these temperatures, but was not observed for LSM at 700 or 800 °C. Comparison of the behavior for LSM and LSCF to the single element oxides provided evidence that Mn and Co oxide, respectively, dominate the Cr contamination of these catalyst materials. This work indicates that a chemical pathway for Cr contamination exists, the effects of which can be minimized by lowering the SOFC operating temperature. The results presented here do not exclude the possibility of enhanced Cr deposition via an electrochemical pathway in an operating SOFC.

Chromium diffusion out of the stainless steel contact particles was seen to affect Cr_2O_3 scale formation. It is not yet clear whether this is detrimental to the long-term oxidation stability of the stainless steel.

Acknowledgements

The authors gratefully acknowledge the assistance of Grace Lau for sample preparation.

This work was supported in part by the U.S. Department of Energy under Contract No. DE-AC03-76SF00098.

References

[1] S.P.S. Badwal, R. Deller, K. Foger, Y. Ramprakash, J.P. Zhang, Solid State Ionics 99 (1997) 297–310.
[2] S.C. Paulson, V.I. Birss, J. Electrochem. Soc. 151 (2004) A1961–A1968.
[3] S. Taniguchi, M. Kadowaki, H. Kawamura, T. Yasuo, Y. Akiyama, Y. Miyake, T. Saitoh, J. Power Sources 55 (1995) 73–79.
[4] Y. Matsuzaki, I. Yasuda, J. Electrochem. Soc. 148 (2001) A126–A131.
[5] S.P. Jiang, J.P. Zhang, X.G. Zheng, J. Euro. Ceram. Soc. 22 (2002) 361–373.
[6] S.P. Jiang, S. Zhang, Y.D. Zhen, Mater. Sci. Eng. B 119 (2005) 80–86.
[7] K. Hilpert, D. Das, M. Miller, D.H. Peck, R. Weiβ, J. Electrochem. Soc. 143 (1996) 3642–3647.
[8] H. Kurokawa, C.P. Jacobson, L.C. DeJonghe, S.J. Visco, Solid State Ionics, submitted for publication.
[9] J.W. Fergus, Mater. Sci. Eng. A 397 (2005) 271–283.
[10] B.B. Ebbinghaus, Combust. Flame 93 (1993) 119–137.
[11] C. Gindorf, L. Singheiser, K. Hilpert, J. Phys. Chem. Solids 66 (2005) 384–387.
[12] A.N. Hansson, S. Linderoth, M. Mogensen, M.A.J. Somers, J. Alloys Compd. 402 (2005) 194–200.
[13] W. Qu, L. Jian, J.M. Hill, D.G. Ivey, J. Power Sources 153 (2006) 114–124.
[14] P. Decorse, G. Caboche, L.-C. Dufour, Solid State Ionics 117 (1999) 161–169.
[15] L.C. DeJohnge, C.P. Jacobson, S.J. Visco, in: M. Mogensen (Ed.), Sixth European Solid Oxide Fuel Cell Forum Proceedings, European Fuel Cell Forum, Oberrohrdorf, Switzerland, 2004, pp. 91–94.